JOURNAL OF APPLIED PHYSICS **117**, 015901 (2015)

Generation of fast cumulative water jets by underwater electrical explosion of conical wire arrays

D. Shafer, V. Tz. Gurovich, D. Yanuka, E. Zvulun, S. Gleizer, G. Toker, and Ya. E. Krasik
Physics Department, Technion, Haifa 32000, Israel

(Received 12 November 2014; accepted 24 December 2014; published online 6 January 2015)

The results of experiments with underwater electrical explosion of conical arrays of copper wires are presented. A pulsed generator producing a 300 kA-amplitude current with a 1.2 μs rise time was used in the explosion of the arrays. As a result of the explosion, fast-moving water jets, with velocities of up to 1200 m/s, were observed being ejected from the surface of the water covering the wire array. The position of the water jets was measured by multiple-exposure fast framing imaging. The apex angle of the array or the thickness of the water layer above the arrays was altered from shot to shot, which changed the resulting velocities and shapes of the emitted jets. A numerical model, based on the models of cumulation and penetration of a jet through material of similar density, is suggested. The velocities of jets obtained by this model agree well with the experimentally observed jet velocities. © *2015 AIP Publishing LLC*. [http://dx.doi.org/10.1063/1.4905548]

I. INTRODUCTION

The phenomenon of water jets generated as a result of underwater explosions of different explosives in the vicinity of the water surface (shallow underwater explosions) has been known since as early as the beginning of the 20th century. Since then, many experimental and theoretical studies were devoted to this subject and the main results are summarized in textbooks.[1,2] In order to observe the generated jets, framing cameras were placed above and under the surface of the water. The framing images acquired by the cameras placed underwater showed that the explosion produces a shock wave (SW), the front of which roughly reproduces the initial shape of the explosive charge. This SW expands, reaches the surface of the water, and refracts from it. At the location of the explosive charge, one obtains the formation of a cavity, which also expands. The reflected SW reaches this cavity and re-refracts from it. In turn, the cavity experiences collapse because of the pressure of the surrounding water. The framing images obtained by the camera positioned above the water showed that, after a certain time with respect to the beginning of the explosion, the free surface of the water becomes concave. At that time, a fast-rising water jet emerges from the water surface. It was observed that this fast rising jet has a diameter smaller and a height larger than the depth of the charge.

Several models have been proposed to explain this phenomenon, two of which provided the most reasonable explanations.[3,4] Both of these models assume that the role of the cavity in jet formation is crucial, the incompressibility of water, and that the role of the SW in the jet formation is negligible. The model described in Ref. 3 considers jet formation due to the interaction between the upper part of the expanding cavity and the free surface of the water. In contrast to this model, the model described in Ref. 4 suggests a hypothesis that the lower part of the cavity deforms in such a way that an upward-moving cumulative jet is generated, which perforates the free water surface. The results of experimental research, with different masses of explosive charges placed at different depths and with different modeling showed that, indeed, the cavity plays a crucial part in the jet formation, the jet dynamics can be simulated within the framework of a model of an incompressible fluid, and the impact of the SW on the jet formation is negligible. The jet generation can be considered a cumulation process,[5] namely, the increase in the density of water in some confined space due to dynamic evolution of the cavity, which leads to the acquisition of a substantial vertical velocity by the jet.

A similar phenomenon of cumulation is obtained in the case of hollow explosive charges.[6] In this approach, a cone-shaped cavity is formed by a thin sheet of metal having a relatively low melting point, with a slab of high explosives attached to its external part. The detonation of the explosive material causes the sheet to be accelerated toward the cavity's axis, where it collapses. This leads to the formation of two cumulative jets, namely, a fast, thin, axis-directed jet moving toward the basis of the cone, and a slower, thicker jet moving in the opposite direction. This process can be described by a model of an incompressible fluid.

Recently, experimental research showed that the underwater electrical explosion of either cylindrical[7] or spherical[8] wire arrays can be used to generate converging strong SW, characterized by pressure values of $>10^{11}$ Pa behind the SW front in the vicinity of either the implosion axis or the origin. In the present paper, the results of experiments with underwater electrical explosion of conical wire arrays, which generate converging strong SW and cumulative water jets, are described. These fast jets penetrate the water layer above the array and emerge into the air above the water surface. In the "Discussion," the model describing the process of the compression of water by the explosion of a conical wire array, the generation of the water jet, and its penetration of the water layer above the cone and emergence into the air, is presented. There is satisfactory agreement between the calculated and the measured values of the velocity of the jet for different geometries of cones.

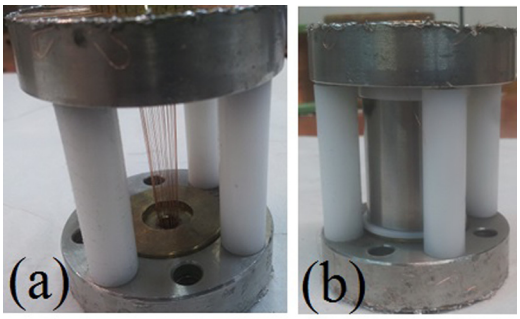

FIG. 1. External view of the arrays without (a) and with (b) a reflector.

II. EXPERIMENTAL SETUP

The cone wire array was constructed of 40 copper wires, each being 0.1 mm and ~40 mm in diameter and length, respectively. The wires were stretched between two circular brass electrodes of different diameters (see Fig. 1 and Table I), thereby allowing the apex angle of the conical array to be varied. A hollow stainless-steel reflector was placed around the wire array, in order to reflect part of the SSW, which was expanding outward, back to the axis.[9] This reflector had the same apex angle as the wire array and it was connected to the high-voltage electrode. A plastic insert, 2 mm in thickness, was used to prevent a discharge between the reflector and the grounded electrode.

The wire array was placed in a de-ionized water-filled, stainless-steel chamber with windows for optical observations. An expanded beam of a 40 mW continuous wave 532 nm laser was used for back-lighting (see Fig. 2). The wire array's location resembled a "V," i.e., its apex was pointing down, toward the high-voltage electrode, and the cone base was just below the level of the windows (see Fig. 3). A fast framing 4QuikE camera (Stanford Computer Optics) was used to acquire the shadow images of the generated jet propagating in air.

The wires were exploded by a current pulse with an amplitude of ~270 kA and rise time of ~1.2 μs supplied by a high-current pulse generator[10] charged up to 27 kV (stored energy of ~3.6 kJ). During the explosion, each wire produced its own cylindrically expanding SW. At some typical distance (roughly equal to the distance between the wires axes), the neighboring SWs overlap with each other, thus forming a single converging conical SSW, similar to that obtained in experiments with cylindrical wire arrays.[7] One can consider this converging conical SW to be a source of the axis-directed water flow behind the SW front. The implosion of this azimuthally symmetrical water flow at the axis of the cone generates an upward-directed water jet. The latter is accelerated toward the top of the cone, penetrates the water layer above the cone, and is ejected into the open air. The thickness of the water layer was varied in the range of 1–6 mm in order to examine the influence of the thickness on the jet velocity.

TABLE I. The combinations of the inner diameters of the conical array electrodes and the resulting apex angles.

Type of array	Ground electrode holder diameter (mm)	High-voltage electrode holder diameter (mm)	Resulting cone apex angle (deg)
Conical	20	5	$2\theta_{03} = 21.24$
Conical	12	2.5	$2\theta_{02} = 13.54$
Conical	10	5	$2\theta_{01} = 7.16$
Cylindrical	12	12	$2\theta = 0$

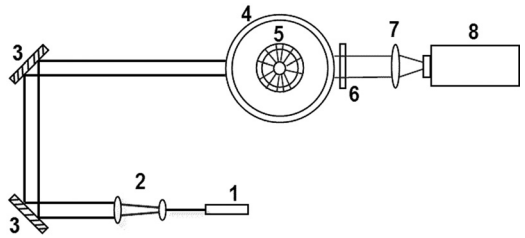

FIG. 2. Optical setup. (1) 40-mW CW 532 nm laser; (2) beam expanding lenses; (3) aluminized mirrors; (4) experimental chamber; (5) conical wire array (top view); (6) 532 nm narrow (1 nm) band-pass filter; (7) focusing objective; (8) fast framing camera 4QuickE.

A spatial calibration was carried out prior to the experiments, using an optical target (see Fig. 4) placed at the location where the jet was expected to arrive during the experiment, i.e., at the axis of the cone just above the wire array. Prior to each experiment, an image of this optical target was obtained, providing the spatial conversion ratio between the observed dimensions of the jet in pixels on the screen of the 4QuikE camera and the actual size in millimeters.

After its emergence into the air, the fast water jet blocks part of the back-lighting beam. This results in a shadow image or a series of images recorded by the 4QuikE camera. In Fig. 5, one can see the tip of the fast jet emerging into the air (a dark shadow just above the water) and the fast SW generated in air by this jet (a thin Gaussian-shaped shadow). These shadow images, together with the simultaneous acquisition of the times at which each frame was obtained with respect to the beginning of the discharge current, allow the calculation of the time-of-flight (TOF) of both the jet and the SW that precedes it. Thus, when a multiple exposure image (several overlaid frames of 5 ns time duration each and time delay between frames of several μs) was obtained, the velocity of the SW and of the jet could be deduced (see Figs. 7 and 8 in Sec. III).

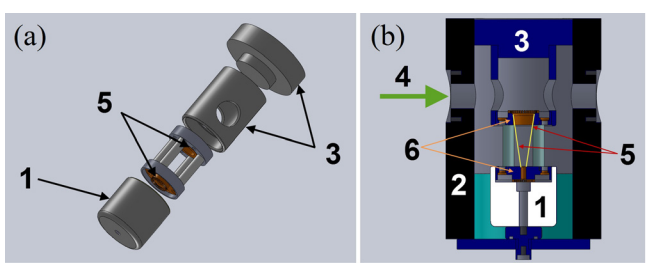

FIG. 3. Assembly of the conical wire array holder without a reflector (a) and its alignment in the experimental chamber (b). (1) High-voltage electrode; (2) experimental chamber; (3) ground electrode with cylindrical holder of the wire array; (4) the direction of the incoming backlight laser beam; (5) conically aligned wires of the array (yellow lines indicated by red arrows); (6) brass electrodes holding the wires (orange parts indicated by orange arrows).

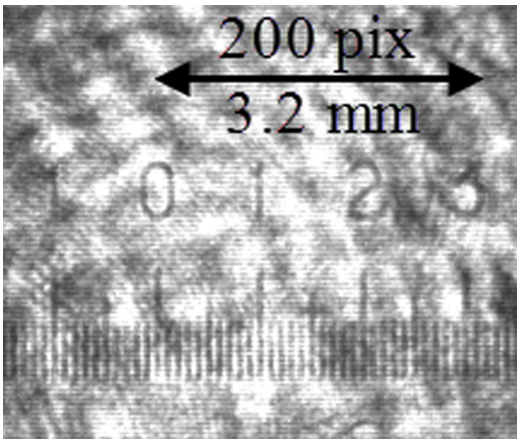

FIG. 4. Image of the transparent ruler used for the spatial calibration. The ruler was placed just above the wire array.

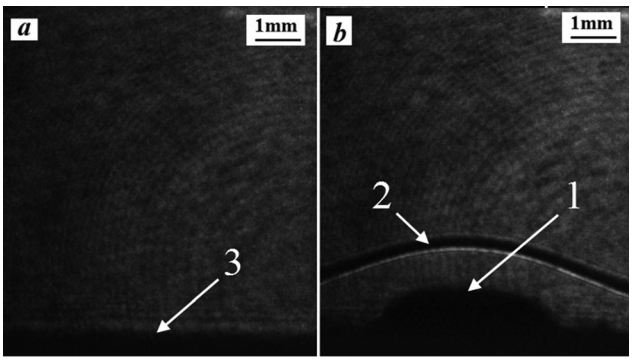

FIG. 5. A single-exposure shadow image prior to (a) and after (b) the explosion of a wire array with a reflector. (1) Fast jet; (2) SW in air; (3) water surface before the experiment. Frame duration of 4QuikE camera is 5 ns.

The discharge current $I(t)$ and the voltage $\varphi(t)$ waveforms were measured using a self-integrated Rogowski coil and a Tektronix P6015A high-voltage probe, respectively. These data were acquired by a Tektronix TDS2024 4-channel digital oscilloscope, together with the synchronization output signal of the 4QuikE camera. In order to calculate the energy deposited into the exploding wires, the resistive voltage V_R on the wire array was calculated by subtracting the inductive component from the measured voltage $V_R = \varphi(t) - L[dI(t)/dt]$, where L is the array inductance. The array inductance was obtained in experiments with a short-circuit load, which was a cylindrical metal slab with physical dimensions similar to those of the wire array. Subsequently, the power was calculated according to $P(t) = V_R(t)I(t)$ and the total energy deposited into the wire array over the time of the discharge by $E = \int_{t=0}^{t_F} P(t)dt$, where t_F is the time when the discharge current is terminated (see Fig. 6 in Sec. III).

III. RESULTS

Typical waveforms of the discharge current and of the voltage, together with the power and the energy deposited into the exploding wires, are shown in Fig. 6. One can see that the wire array explosion occurs at an amplitude of the discharge current of ~220 kA (current density in each wire ~68 MA/cm^2). This explosion can be characterized as an aperiodical discharge, since ~70% of the stored energy is deposited into the exploding wire during ~700 ns. The wire array resistance at the maximum of the peak power of 9 GW reaches ~0.2 Ω (resistance of each wire reaches, respectively, ~8 Ω).

During the experiments, the snapshots of the generated jets were captured by a 4QuikE camera with varying time delays in the range of 6–22 μs with respect to the beginning of the discharge current. It was observed that there are slight variations in shape of the jets and SWs between different experiments. Therefore, only the data from multiple-exposure shots were analyzed, allowing us to disregard these variations, as well as the time jitter of wire explosion. The results of experiments where the apex angle of the array was fixed at $2\theta = 7.16°$, while the water layer thickness was varied in the 1–6 mm range, and experiments where the water layer thickness was not varied, while wire arrays with varying apex angles were exploded, are presented in Table II. A set of experiments with a varying level of water covering the array were performed in order to investigate the influence of the thickness of the water layer that the jet penetrates before it emerges into the air. The purpose of the series of the experiments where only the apex angles were varied was to examine the influence of the angle on the velocity of the emerging jet and its shape.

The data obtained for these series are shown in Figs. 7 and 8. One can see that all the data points are linearly aligned, which means that the velocities of both the jets and the SWs propagating in air are constant. The fastest jet and SW originate in the setup with the lowest water layer thickness, namely, 1 mm, where the velocity of the jet reaches 1.25×10^5 cm/s. This result can be qualitatively explained by the smallest thickness of the water layer that the jet has to penetrate. One can see the 2-exposure overlaid image obtained in this particular experiment in Fig. 9. The jet's shape is almost perfectly conical, without a visible SW in front of the jet. The jet seems to "slice through" its SW, and the part of the SW in front of the jet is missing. This can be explained by the high velocity of the jet, which is sufficiently

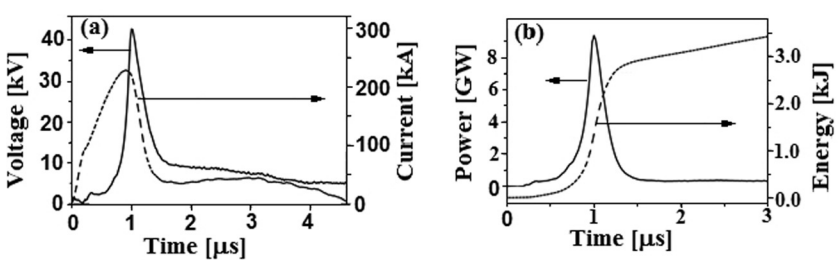

FIG. 6. Typical current and resistive voltage (a) during the explosion of wire arrays, and the power and deposited energy (b). The conical wire array is constructed of 40 Cu-wires, each 0.1 mm and ~40 mm in diameter and length, respectively.

TABLE II. Summary of experimental results.

Type of array	Cone apex angle (deg)	Depth of the water level (mm)	Velocity of the jet ($\times 10^5$ cm/s)	Velocity of the SW ($\times 10^5$ cm/s)
Conical	$2\theta_{01} = 7.16$	1	1.25	1.21
Conical	$2\theta_{01} = 7.16$	2	0.53	0.54
Conical	$2\theta_{01} = 7.16$	4	0.55	0.59
Conical	$2\theta_{01} = 7.16$	6	no jet	0.58
Conical	$2\theta_{02} = 13.54$	4	0.76	0.75
Conical	$2\theta_{03} = 21.24$	4	0.91	0.87
Cylindrical	$2\theta = 0$	2,4,6	no jet	0.4

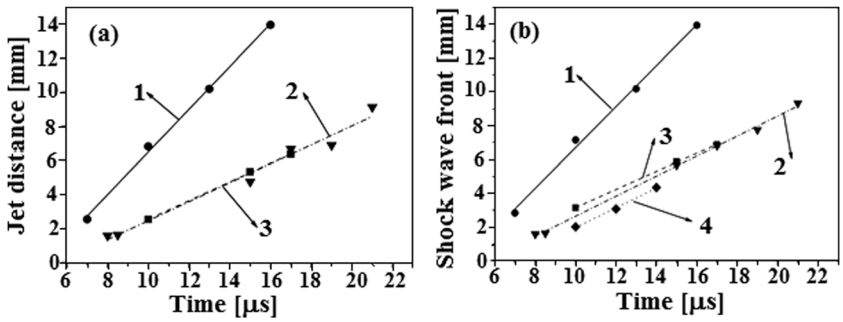

FIG. 7. The measured TOF and distance of the jets (a) and of the shockwaves (b) from the surface of the water in the series where only the water layer thickness was varied. The same wire array with apex angle of $2\theta = 7.16°$ was used. (1) 1 mm water layer, $V_{jet} = 1.25 \times 10^5$ cm/s, $V_{SW} = 1.21 \times 10^5$ cm/s. (2) 2 mm water layer, $V_{jet} = 0.53 \times 10^5$ cm/s, $V_{SW} = 0.54 \times 10^5$ cm/s. (3) 4 mm water layer, $V_{jet} = 0.55 \times 10^5$ cm/s, $V_{SW} = 0.59 \times 10^5$ cm/s. (4) 6 mm water layer, $V_{SW} = 0.54 \times 10^5$ cm/s; no jet was observed.

fast to engulf its own SW. The TOF analysis, together with the measurement of the dimensions of the jet in this image, allows a rough estimate of the kinetic energy carried by this jet, $E_{\text{jet}} \approx 7$ J.

In the experiments with 2 mm and 4 mm water layer thicknesses and the same cone apex angle of $2\theta = 7.16°$, the velocities of the jets and the accompanying SWs decrease by ~2.3 times as compared with their values for the 1 mm water layer thickness. At the greatest water layer thickness of 6 mm tested in this research, the jet is no longer observed and only the SW is visible. One can suppose that in this configuration the energy of the jet was just sufficient for it to penetrate the water above the array, but not sufficient for it to emerge above the water layer.

Fig. 8 shows that the velocities of both the jet and the SW increase with the cone apex angle for the angle values tested in this study. This result will be discussed in detail in Sec. IV.

A typical multiple-exposure shot of a single experiment is presented in Fig. 10. One can see the narrow column of the jet, propagating upward. An SW preceding the jet is generated because of the jet's supersonic movement in air. One can see the Mach cone of the SW and the rest of the SW swept aside from the jet. These data allow one to apply an additional evaluation method of the jet velocity. Indeed, it is well-known that an object propagating with supersonic velocity V in a medium where the sound velocity is C_S generates an SW with a Mach cone characterized by the angle $\sin\theta = C_S/V$.[11] Thus, using the measured Mach cone angle of $\theta = 41.3°$ and the velocity of sound for air $C_S = 330$ m/s, one obtains a jet velocity of $V \approx 0.5 \times 10^5$cm/s, which is consistent with the TOF measurements (see Table II).

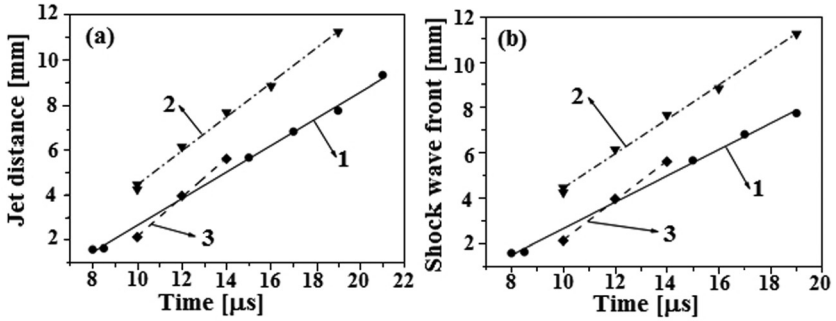

FIG. 8. The measured TOF and distance of the jets (a) and of the shockwaves (b) from the surface of the water in the series where only the apex angle of the array was varied. The water layer thickness was 4 mm. (1) $2\theta = 7.16°$, $V_{jet} = 0.55 \times 10^5$ cm/s, $V_{SW} = 0.59 \times 10^5$ cm/s. (2) $2\theta = 13.54°$, $V_{jet} = 0.76 \times 10^5$ cm/s, $V_{SW} = 0.75 \times 10^5$ cm/s. (3) $2\theta = 21.24°$, $V_{jet} = 0.91 \times 10^5$ cm/s, $V_{SW} = 0.87 \times 10^5$ cm/s.

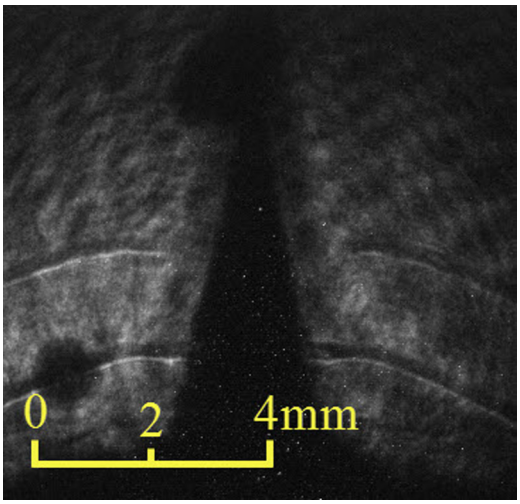

FIG. 9. The two-exposure image of the jet originating from the explosion of an array with an apex angle of $2\theta = 7.16^\circ$ and water layer thickness of 1 mm. The frames were taken at $t_1 = 14\,\mu$s and $t_2 = 16\,\mu$s. One can see the conical shape of the jet with no visible shock wave in front of it.

IV. DISCUSSION

In this section, a steady-state model of water compression caused by the electrically exploding conical-shaped plasma shell is discussed. The model considers a metallic rigid cone, the length of the side of which is $R_0 = l$ and half of the apex angle is θ_0 (see Fig. 11). A conical wire array with the same length and angle as the cone is placed inside the cone in close proximity to the metal wall. In order to simplify the calculation of the array explosion, it is assumed that the explosion is characterized by a constant energy deposition rate, w, and that the energy deposited into the array is equally distributed along the length of the wires. In addition,

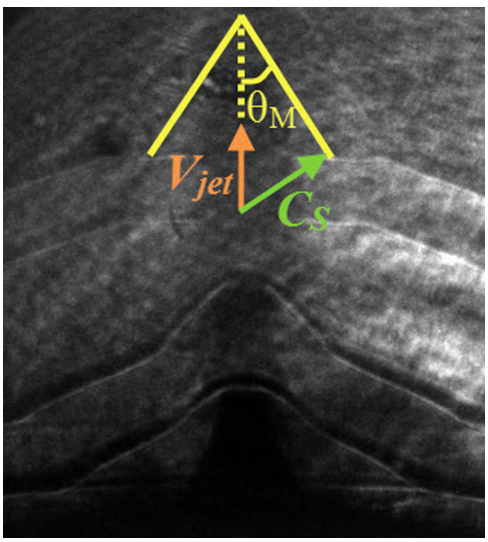

FIG. 10. Typical four-exposure image of the jet and SW in air. The apex angle of the wire array is $2\theta = 7.16^\circ$ with a water layer thickness of 4 mm. Note the blunt "nose" of the emerging jet and the Gaussian-shaped shock wave with the clearly visible Mach cone. Color marking code of snapshot taken at $t = 18\,\mu$s: orange—direction of the flight of the jet; green—direction of the sideways expansion of the sound wave in air; yellow—marking of the Mach cone with its angle.

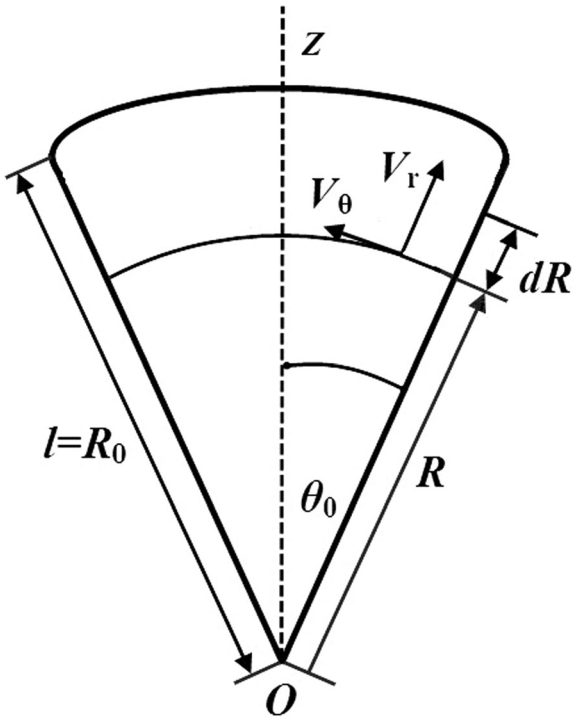

FIG. 11. The coordinates of the theoretical model.

it is supposed that a thin plasma cone with a width of $d \ll l$ is formed when the number of wires is $N \gg 1$. In the case of a 40-wire conical array, with a base radius of 5 mm, consisting of copper wires 0.1 mm in diameter, one obtains that, at $\sim 2\,\mu$s with respect to the beginning of wires explosion, a conical plasma shell should be formed because of the radial expansion of the wires with a velocity of $\sim 10^5$ cm/s.[12]

A spherical system of coordinates, with its center coinciding with the apex of the cone, presenting a part of a sphere and with the OZ axis lying along the symmetry axis of the cone, is considered. An elementary volume of the plasma shell, $dV = (dS)d$, absorbs the energy of $Nw(dR/l)$ from N exploding wires at any given instant. Here, $dS = 2\pi R \sin\theta dR$ is the unit area of the cone. Thus, one obtains that the energy density dW in the volume unit (i.e., the pressure P) in the vicinity of the wall depends on the radius as $dW \approx Nw\ (dR/l)/(dS)d \propto 1/R$. The model considers a steady state process with an established pressure distribution and the flow of low-compressible water inside the cone. The assumption of non-compressibility of water means that the increase in the water density has been neglected, i.e., the water flow has been considered in the acoustic approximation. The system of Euler equations for an incompressible fluid reads[11]

$$\frac{\partial \vec{v}}{\partial t} + (\vec{v} \cdot \vec{\nabla}) \cdot \vec{v} = -\vec{\nabla}\left(\frac{P}{\rho}\right), \quad \vec{\nabla} \cdot \vec{v} = 0.$$

In the case of the azimuthal symmetry, V_r and V_θ are the only non-zero components of the water flow velocities. The system of discontinuity and Euler equations for these non-zero velocity components of the liquid, written with a dimensionless coordinate $r = R/l$, reads

$$\frac{1}{r^2}\frac{\partial(r^2V_r)}{\partial r}+\frac{1}{r\sin(\theta)}\frac{\partial(V_\theta\sin\theta)}{\partial\theta}=0,$$
$$V_r\frac{\partial V_r}{\partial r}+\frac{V_\theta}{r}\frac{\partial V_r}{\partial\theta}-\frac{V_r^2}{r}=-\frac{1}{\rho_0}\frac{\partial P}{\partial r}, \quad (1)$$
$$V_r\frac{\partial V_\theta}{\partial r}+\frac{V_\theta}{r}\frac{\partial V_\theta}{\partial\theta}+\frac{V_rV_\theta}{r}=-\frac{1}{\rho_0 r}\frac{\partial P}{\partial\theta}.$$

Here, $P(r,\theta)$ is the pressure inside the water. Now, by using dependence of pressure versus radius as $P \propto 1/r$, a self-similar solution of Eqs. (1) can be searched as

$$V_r = V_0\Re(\theta)/\sqrt{r},$$
$$V_\theta = V_0\Theta(\theta)/\sqrt{r}, \quad (2)$$
$$P = \rho_0 V_0^2\Pi(\theta)/r.$$

Here, V_0 is the typical velocity of the water jet, which will be defined later. $\Re(\theta)$, $\Theta(\theta)$, and $\Pi(\theta)$ are dimensionless functions,[13] which depend on the azimuthal angle θ only. These functions are the self-similar representatives of water flow parameters V_r, V_θ, and P, and they can be found by solving Eq. (3), after substitution of expressions (2) in Eq. (1)

$$\frac{d\Theta}{d\theta}=-3\Re/2-\Theta ctg(\theta),$$
$$\frac{d\Pi}{d\theta}=\Theta[\Re+\Theta ctg\theta], \quad (3)$$
$$\Theta\frac{d\Re}{d\theta}=\Pi+\Theta^2+\Re^2/2.$$

Equation (3) is a system of ordinary differential equations (ODEs) with three unknown variables, Θ, Π, and $\Re$, and with boundary conditions determined by the symmetry of the water flow. The solution of Eq. (3) allows the physical variables to be calculated by multiplying dimensionless functions Θ, Π, and $\Re$ by their appropriate dimensional parameters [see Eq. (2)]. The boundary conditions at the OZ axis (at $\theta=0$) require that the velocity component $V_\theta=0$ and the derivative of the pressure $dP/d\theta=0$, and that at $\theta=\theta_0$, $V_\theta=0$. By using Eq. (2), the water flux through some arbitrary part of the spherical surface defined by r inside the cone can be estimated as

$$J(r)=2\pi\rho_0\int_0^{\theta_0} r^2V_r(r,\theta)\sin\theta d\theta$$
$$=2\pi\rho_0V_0r^{3/2}\int_0^{\theta_0}\Re(\theta)\sin\theta d\theta. \quad (4)$$

In the case of a steady-state water flow, this flux should be constant for any r. However, one sees that this flux depends explicitly on r. This contradiction can be resolved by the requirement that the integral in Eq. (4) be zero. This can be satisfied only if the radial component of the water flow velocity, V_r, changes its sign (i.e., the direction of the water flow) at some critical angle θ_{cr}. Thus, in addition to the boundary conditions, one obtains the condition for a constant water flow

$$\int_0^{\theta_0}\Re(\theta)\sin\theta d\theta=0. \quad (5)$$

The boundary conditions at the vicinity of the OZ axis, which are required for the solution of Eq. (3), are obtained by analyzing the analytical solution of Eq. (3) in this region. This solution can be obtained by making several approximations for the dimensionless functions. At $\theta\to0$, the value of V_θ, and accordingly of $\Theta(\theta)$, approaches zero, $ctg\theta$ approaches infinity, and the derivate of the pressure is almost zero. Thus, at $\theta\to0$, the following inequality between the dimensionless functions exists:

$$\Re\gg\Pi\approx1\gg\Theta.$$

This inequality, together with the definition of the dimensionless representative functions [see Eq. (2)], allows Eq. (3) to be rewritten as

$$\Re+\Theta ctg\theta\approx0,$$
$$d\Theta/d\theta=-\Re/2, \quad (6)$$
$$d\Re/d\theta=\Re^2/2\Theta.$$

The solutions for $\Theta(\theta)$ and $\Re(\theta)$ reads

$$\Theta=C\sqrt{\sin\theta}\quad \Re=-C\cos\theta/\sqrt{\sin\theta}. \quad (7)$$

Here, C is the integration constant. These solutions allow us to determine the boundary conditions for $\theta_1\ll1^\circ$, which are necessary for the numerical solution of Eq. (3). Let us note that Eq. (3) does not change when $\Pi\to C^2\Pi$, $\Re\to C\Re$, and $\Theta\to C\Theta$. This was used for the solution of Eq. (3). Namely, for a certain value $\theta_1\ll1^\circ$, the initial values of $\Re(\theta_1)$ and $\Theta(\theta_1)$ are calculated by using the analytic solutions (7) with the value of the constant $C=1$. For the same value θ_1, an arbitrary positive value for $\Pi(\theta_1)$ was chosen. For these boundary conditions, namely, for the known values of $\Re(\theta_1)$, $\Theta(\theta_1)$, and $\Pi(\theta_1)$, the distributions of $\Re(\theta)$, $\Theta(\theta)$, and $\Pi(\theta)$ were determined using the numerical solution of Eq. (3). The next step was the calculation of the integral (5) with the known distribution of $\Re(\theta)$. In the case where this integral is not zero, a new value of $\Pi(\theta_1)$ was selected and the procedure was repeated until condition (5) was satisfied. The final iteration, i.e., when condition (5) was satisfied, showed that the representative of velocity $\Theta(\theta)$ approaches almost zero at $\theta=\theta_0$, which agrees with the condition of $V_\theta=0$ at that location. In addition, let us note that the obtained distribution of the representative function of pressure $\Pi(\theta)$ was found to be almost constant. Thus, the only significant pressure gradient exists along r, i.e., in the vertical direction.

In the experiments, three wire arrays with apex angles of $\theta_{01}=3.58^\circ,\theta_{02}=6.79^\circ,\theta_{03}=10.62^\circ$, base radii of $r_1=5\,\text{mm}$, $r_2=6\,\text{mm}$, $r_3=10\,\text{mm}$, and side lengths of $(l_i=r_i/\sin\theta_i;i=1,2,3)$ $l_1\approx80\text{mm},l_2\approx51\text{mm},l_3\approx54\text{mm}$, respectively, were tested. For these arrays, the set of parameters Π_i, which were found to satisfy condition (5) are $\Pi_1\approx18.4778$, $\Pi_2\approx9.7116$, and $\Pi_3\approx6.1187$, respectively. The critical angles for these parameters, i.e., the angles at which the direction of the water flow is reversed and for

which the representatives of radial velocities $\Re_i(\theta_{cr})=0$, are $\theta_{cr1}=2.39°$, $\theta_{cr2}=4.56°$, and $\theta_{cr3}=7.41°$, respectively. These angles also determine the maximal radii of the cross section of the ejected jets at the base of the array cone of 3.4 mm, 4.1 mm, and 7 mm, respectively.

Finally, in order to obtain values $V_r(r)$, $V_\theta(\theta)$, and $P(r,\theta)$ for the determined distributions $\Re(\theta)$, $\Theta(\theta)$, and $\Pi(\theta)$, one has to determine the value of the typical velocity V_0 of the water flow [see expressions (2)]. The latter can be obtained using the calculation of the net flux of the kinetic energy of the water flow through the base of the array

$$W = 2\pi\rho V_0^3 l^2 S_e. \tag{8}$$

Here, $S_e = \frac{1}{2}\int_0^{\theta_0} [\Re(\theta)]^3 \sin(\theta) d\theta$ is computed by using the obtained distribution of $\Re(\theta)$. The non-zero value of S_e is related to the net outflowing kinetic energy flux of the water jet. This energy flux W can be estimated using the measured power $P_E \approx 9\times10^9$ W deposited into the wire array, multiplied by the efficiency of the conversion of the electrical energy into the energy of the converging water flow $\eta \approx 0.1$.[12,14] The latter allows one to calculate the typical velocity of the jets and the pressure near the cone aperture for the three wire arrays tested. For the first array, $\theta_{01} = 3.58°$: $V_{01} \approx 1218$ m/s, $P_1 \approx 2.74\times10^{10}$ Pa; for the second array, $\theta_{02} = 6.79°$: $V_{02} \approx 1441$ m/s, $P_2 \approx 2.02\times10^{10}$ Pa (this value of the velocity is near the upper value for the valid velocities of this model, since in this model $V_0 < C_S \approx 1500$ m/s); for the third array, $\theta_{03} = 10.62°$: $V_{03} \approx 1268$ m/s, $P_3 \approx 9.85\times10^9$ Pa.

Now, let us compare the results of the experiment with the calculation results in the framework of this model. The velocity of the emerging jets under the assumption of the "incompressibility" of the medium is $U_i \approx V_{0i}/2$.[15] This velocity is acquired by the jet after it has penetrated a water layer with a thickness of $H > H_C$, where H_C is some thickness of water where a stationary penetrating jet is formed. The experiment provides the measurement of the velocity of the jets after they have penetrated water layers of varying thickness H. Thus, in the case of $H \ll H_C$, the value of the jet velocity is close to its value near the aperture of the wire array, and in case $H > H_C$, the jet velocity is $U_i \approx V_{0i}/2$. In the cases where the thickness is intermediate, the values of the velocity will be in the range of $V_{0i}/2 < U_i < V_{0i}$. For the array with apex angle $2\theta_{01} = 7.16°$ and $H = 1$ mm, the calculated velocity is 1250 m/s, close to the measured velocity of $V_{01} \approx 1218$ m/s (see Table II). In the cases of $H = 2$ mm and $H = 4$ mm, the experimentally measured velocities were 530 m/s and 550 m/s, respectively. These velocities are within 10% of $V_{01}/2$, which is also in good agreement with the model.[15] A similar satisfactory agreement was obtained for the array with $2\theta_{02} = 13.54°$ $H = 4$ mm, and a measured jet velocity of ~760 m/s. In this case, water flow velocity calculated at the aperture of the array is $V_{02} \approx 1441$ m/s. Finally, for the wire array with the largest apex aperture angle, $2\theta_{03} = 21.24°$ and $H = 4$ mm the measured velocity is ≈910 m/s. The assumption of $H > H_C$ in this case results in $2U_3 \approx 1820$ m/s, which is substantially larger than the sound speed in water, and the calculated velocity of $V_{03} \approx 1268$ m/s. Therefore, one can conclude that $H < H_C$ for this apex angle.

V. SUMMARY

The results of the experiments showed that underwater electrical explosion of conical wire arrays can be successfully used to generate fast jets emerging from water, instead of the commonly used explosives. It was shown that the geometry of conically shaped wire arrays and the thickness of the water layer above the array determine the parameters of the generated water jet emerging from the water. The experimentally obtained velocities of jets were found to be in good agreement with the developed model for the cumulative flows in water, as well with the model of penetration of water by a fast jet.[15]

ACKNOWLEDGMENTS

This research was supported by the Israeli Science Foundation Grant No. 99/12.

[1]R. H. Cole, *Underwater Explosions* (Princeton University Press, Princeton, 1948).
[2]V. K. Kedrinskii, *Hydrodynamics of Explosion—Experiments and Models* (Springer-Verlag, Berlin, 2005).
[3]M. A. Lavrent'ev and B. V. Shabat, *The Problems of Hydrodynamics and their Mathematical Models* (Nauka, Moscow, 1973).
[4]L. V. Ovsyannikov, "On floating of a bubble," in *Some Mathematics and Mechanics Problems* (Nauka, Leningrad, 1970).
[5]E. I. Zababakhin, *Cumulation and Instability* (Snezhinsk, 1998).
[6]W. P. Walters and J. A. Zukas, *Fundamentals of Shaped Charges* (John Wiley and Sons, New York, 1989).
[7]Ya. E. Krasik, A. Grinenko, A. Sayapin, and V. Tz. Gurovich, Phys. Rev. E **73**, 057301 (2006).
[8]O. Antonov, L. Gilburd, S. Efimov, G. Bazalitski, V. Tz. Gurovich, and Ya. E. Krasik, Phys. Plasmas **19**, 102702 (2012).
[9]L. Gilburd, S. Efimov, A. Fedotov-Gefen, V. Tz. Gurovich, G. Bazalitski, O. Antonov, and Ya. E. Krasik, Laser Part. Beams **30**, 215 (2012).
[10]D. Sheftman and Ya. E. Krasik, Phys. Plasmas **18**, 092704 (2011).
[11]L. D. Landau and E. M. Lifshitz, *Fluid Mechanics*, 2nd ed. (Butterworth–Heinemann, Oxford, 1987).
[12]S. Efimov, A. Fedotov, S. Gleizer, V. Tz. Gurovich, G. Bazalitski, and Ya. E. Krasik, Phys. Plasmas **15**, 112703 (2008).
[13]G. I. Barenblatt, *Scaling, Self-similarity, and Intermediate Asymptotics* (Cambridge University Press, New York, 1996).
[14]A. Grinenko, S. Efimov, A. Fedotov, and Ya. E. Krasik, J. Appl. Phys. **100**, 113509 (2006).
[15]F. A. Baum, K. P. Stanyukovich, and B. I. Shekhter, *Physics of an Explosion* (Department of the Army, Corps of Engineers, 1963).